

Short Communication

Fractal Growth of SiO_x Nanoparticles Accompany with Graphene Preparation

Dongjiu Zhang^{*}, Haifeng Cheng, Zhaoyang Zhang, Yue Kang

National Key Laboratory of Science and Technology on Advanced Ceramic Fiber and Composites, College of Aerospace Science and Engineering, National University of Defense Technology, Changsha, 410073, People's Republic of China.

E-mail: dongjiuz@sina.cn

Received: 11 January 2016 / *Accepted:* 25 March 2016 / *Published:* 4 June 2016

Anisotropic growth mode is generally leading to simple self-similarity patterns. This paper presents a new perspective of looking at SiO_x growth accompanies with graphene growth which is in diffusion-controlled fractal growth process. Growth of SiO_x on the surface of copper was in stages and the samples were constantly monitored by scanning electron microscope. To confirm the critical structure of different etched areas of graphene, Raman spectra as well as energy dispersive spectrum were performed. Morphologies of SiO_x nanoparticles could be controlled by varying the Ar/H₂ flow rate ratios and silica gel concentrations. The characteristic topology of branch-like fractal patterns, identical to the topology of ternary-segment fractal line, is observed.

Keywords: SiO_x Nanoparticles; fractal growth; graphene; diffusion-limited aggregation

1. INTRODUCTION

Nonmetallic SiO_x is an emerging photoluminescence material[1]. Nanoscale SiO_x which are mainly produced by plasma deposition[2] and magnetron sputtering method[3] can be used as quantum dot for light emitting and the color is affected by oxygen content[4, 5]. Besides, nonmetallic SiO_x has been extensively applied in various fields like improving operation of phase change random access memory[6], changing electrical resistance switching in Ti[7], luminescence enhance[8] and so on. Graphene is widely investigated in the field of electronic transistors[9], transparent conductive electrodes[10], energy storage and energy production devices[11] as well as sensor and biosensor[12] due to the one-atom thickness of sp²-hybridized carbon atoms arranging into a hexagonal lattice[13].

As a widespread phenomenon in nature, fractal growth[14-16] which refers to an irregular non-linear system characterizing by self-similarity has already attracted broad attentions and wide applications in various fields of natural sciences like physics[17, 18], chemistry[19], biology[20], materials science[21] and medicine[22] since Mandelbrot[23] proposed fractal theory in 1975. The main application of fractal theory in material science is trying to reveal the physical laws of fractal structure during the nucleation process in the physical processes[24, 25]. It is notable that fractal growth has lots of models[14] and the introduction of simplified models has led to quite a good understanding of the morphology of such growth[17, 26], despite the inapplicability of our usual modes of thinking.

In this article, SiO_x nanoparticles (SiO_x NPs) were prepared by chemical vapor deposition (CVD) method according with fractal growth. During the preparation, monolayer graphene was concomitantly generated and etched. Although the existence of SiO_x was once considered to have negative impact on the synthesis of monolayer graphene[27], uniform and dendrite SiO_x NPs could be successfully prepared, and the etched graphene showed potential applications in non-linear optical and electrical devices. The morphology and structure of SiO_x NPs obtained from different conditions have been studied.

2. EXPERIMENTAL

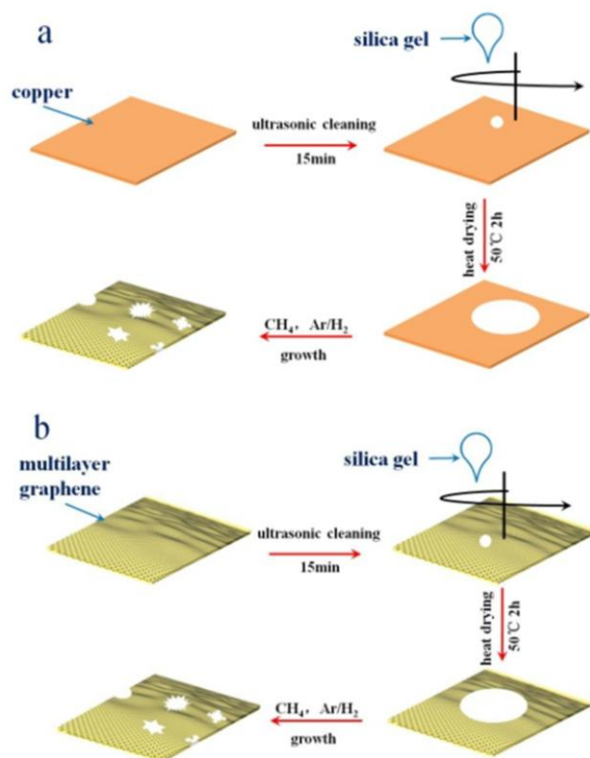


Figure 1. Diagrams showing the process of SiO_x NPs growth on a copper surface (a) Method 1, SiO_x NPs grow with the preparation of single layer graphene; (a) Method 2, SiO_x NPs grow on multilayer graphene

SiO_x NPs with the synthesis of graphene were prepared by the thermal CVD method using Cu foils (Hefei Crystal Technical Material Co. Ltd) as catalytic substrates and silica gel (Momentive) as Si source in two different methods. Detailed operating processes were shown in supporting information (SI).

To survey the intrinsic fractal growth behavior of SiO_x NPs, we started by preparing the films on a copper surface using a recently developed graphene fabrication method. Briefly, half of a Cu substrate was spin-coated with different concentrations of silica gel at 50°C and then placed in a quartz tube to 1060°C. A monolayer graphene film with SiO_x NPs was then grown on the surface of copper using CH₄ in Ar/H₂ as the carrier gas at ambient pressure for different stage (each stage was set for 30minutes). Various Ar/H₂ flow rate ratios were probed to study the effect of the flow rate ratio on the SiO_x nanoparticles pattern. Finally, the sample was cooled rapidly to room temperature (Figure 1a). Another method was that, after the formation of multilayer graphene on Cu foils, silica gel films were coated onto the graphene film by spin coating. Then the Cu foils with silica gel film were heated at 50°C for 2h. After being located in the quartz tube, the samples were heated up to 1060°C with different Ar/H₂ flow rate ratios at ambient pressure. Finally, the sample was rapidly cooled to room temperature (Figure 1b).

3. RESULTS AND DISCUSSION

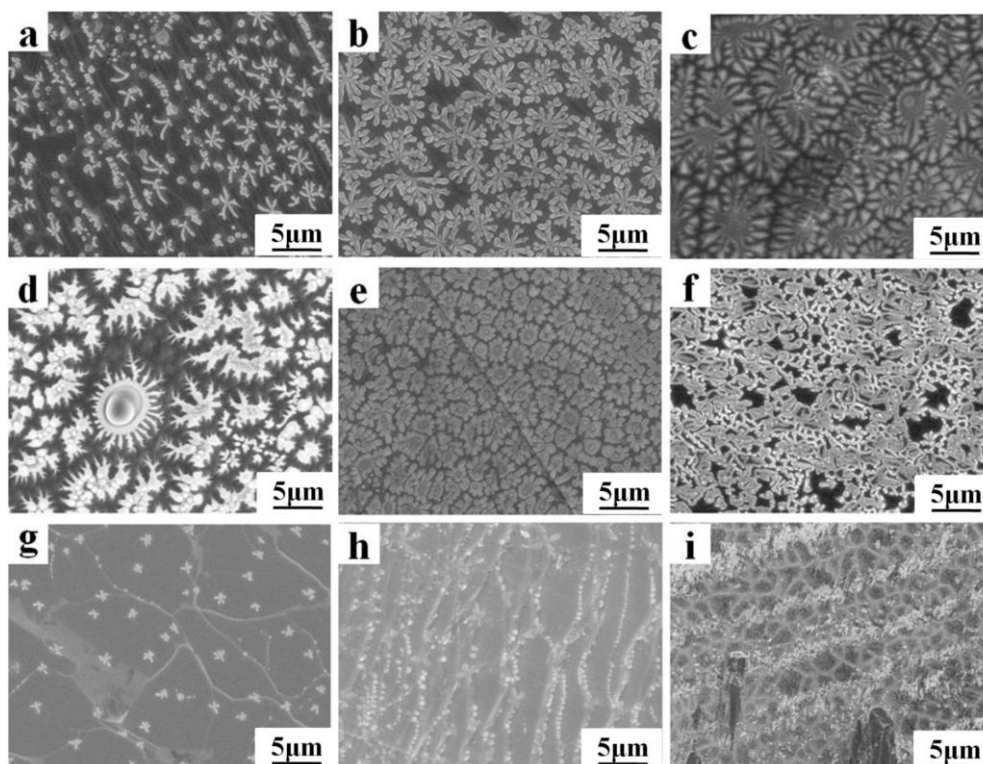


Figure 2. Typical SEM images of SiO_x NPs with different shapes obtained with various silica gel concentration and Ar/H₂ flow rate ratios after etching graphene. The different conditions are summarized in Table S1.

To understand the most favorable structure of SiO_x NPs after etching graphene, a string of typical SEM images of SiO_x NPs patterns obtained from different experimental conditions (Seen in Table S1 in SI) are shown in Figure 2. In all these cases, samples grown with the formation of monolayer graphene (Figure 2a-f) or on the multilayer graphene film (Figure 2g-i) were all prepared on Cu surface employing CH_4 at 0.25 standard cubic centimeters per minute (sccm) and various Ar/ H_2 flow rate ratios at 1060 °C at barometric pressure. The micro morphology examination of these patterns reveals the fractal growth at many different conditions.

When a low Ar/ H_2 flow rate ratio (800 sccm/100 sccm) was exploited in growth stage, sharper branching structure (dendritic structure in Figure 2c) could be observed on the as-grown graphene film (dark area in Figure 2). This observation is similar with those reported previously[28]. At the nucleation state, Si atoms join to form island in the form of ad-dimer[29] which was protected from dissociation by the cohesive energy between the atoms, and atoms diffusing along the island edges were important in controlling the formation of highly anisotropic fractal island[15, 30, 31]. The following growth mode was highly according with the principle of extended fractal growth proposed by Zhang[32]. Namely, the adatoms reaching the edge of island had enough time to find a favorable site where existed at least two nearest neighbors to form a triangular lattice, and then grew up to the branching structure. With the increase of Ar/ H_2 flow rate ratio, the edge of branches started to curve and the end of the branches became broad gradually (Figure 2b). This phenomenon was thought to be that low H radical concentration restrained the movement of adatoms before they were pinned in the position by the arrival of other atoms. When the Ar/ H_2 flow rate ratio increased to a certain level, the dendritic structure seemed to become less clear (Figure 2a). These phenomena, including branching, broadening, curvature and disappearance of protruding parts, are supposed to be the characteristic of diffusion-controlled process. Since silica gel would be degraded during the process of heating up to 1060°C, SiO_x NPs have already existed on the surface of Cu substrate before the formation of graphene. Thus, the etching process along with the growth of SiO_x NPs was started from these points where SiO_x NPs existed. In the process, H_2 or activated H radicals were probably served as active etchants to graphene and promoted the growth of SiO_x NPs. Subsequent etching pathway mainly depended on the competing rates of (1) the etching rates along the points to find the most energetically favorable directions and (2) the diffusion rate of etchants, while too fast diffusion rate of etchants would impede the process of finding the most energetically favorable directions, leading to a branched structure[28]. Therefore, with the decrease of Ar/ H_2 flow rate ratios, a sharp dendritic structure appeared, as seen in Figure 2c.

According to the SEM images (Figure 2d-f), dendritic structure became more and more indistinct as the concentration of silica gel increased. When the concentration was low, the branches with many protruding arms were observed (Figure 2d), but these arms gradually disappeared (Figure 2e) and eventually vanished (Figure 2f) with the increase of the concentration. This was because, high concentration of silica gel led to dense SiO_x NPs which would occupy the space of graphene before sufficient growth. Namely, etching process was limited by the high concentration of SiO_x NPs.

From Figure 2g-i we can clearly figure out that the effect of Ar/ H_2 flow rate ratio on SiO_x NPs morphology showed the same tendency when prepared samples on multilayer graphene as on single layer graphene, but the influence of concentration of silica gel varied greatly. When the concentration

of silica gel was low, the branches were more likely to be flowers without any projecting arms on the multilayer graphene (Figure 2g). With the increase of concentration, almost all of the particles gathered at the edge of graphene layers (Figure 2h), when the concentration reached more than 30%wt, SiO_x NPs agglomerated and formed linear structure and network(Figure 2i). This was probably because the etching was prior to starting from the interaction of NPs and carbon atoms at the edges where atoms were more active than those within the graphene sheet since few vacancies were existed within the surface of graphene sheet due to the perfect graphite crystalline structure with sp²-hybridized carbon atoms being well arranged into the hexagonal lattice[33], but at the boundaries where more vacancies existed, atom Si was easier to form Si-C bond causing the assembling phenomenon of NPs. Similar phenomenon has also been revealed by Geng. etc[26] during the etching process of graphene. These vacancy defects have also been detected in the Raman spectra.

Comparing Figure 2e and 2h, 2f and 2i, respectively, we can find a phenomenon that etching process was much easier on single layer graphene than that on multilayer graphene. Since operating temperature was set at 1060°C near the melting point of Cu, the surface free energy of Cu was higher than that of graphene, etchants were prior to being absorbed and diffused on Cu surface[26]. Therefore, effective etching process was preferential to starting on single layer graphene which had relatively high contact surface with Cu substrate than the multi-one.

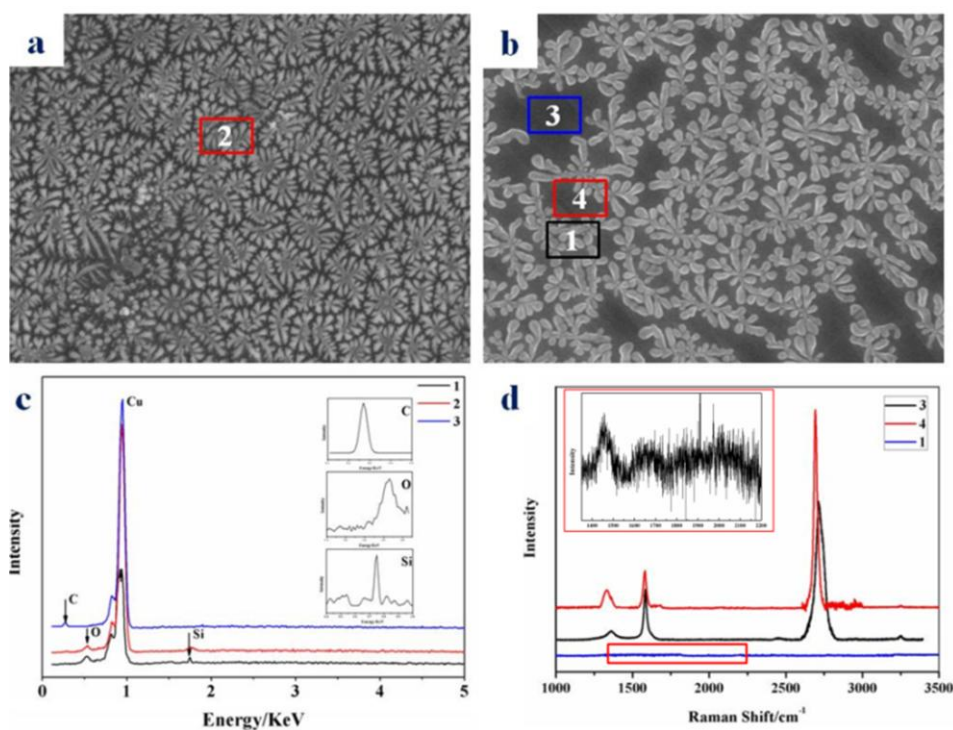


Figure 3. Characterizations of SiO_x NPs structures. (a) SEM images of SiO_x NPs dendritic structure at Low Ar/H₂ flow rate ratio on single layer graphene (b) SEM images of SiO_x NPs dendritic structure at High Ar/H₂ flow rate ratio on single layer graphene. Labels 1 and 2 in (a) and (b) indicate SiO_x NPs regions respectively, labels 3 and 4 indicate graphene film regions after SiO_x NPs etched respectively. (c) EDS spectra of regions 1, 2 and 3 in (a) and (b). (d) Raman spectra of regions 1, 3 and 4 in (b). All scale bars are 10 μm.

The above SiO_x NPs fractal patterns were confirmed by further characterizations. Typical SEM images of a dendritic structure SiO_x NPs (Figure 3a and 3b) show the commonly observed graphene films (the dark area) and the different branches pattern (the white structure). Labels 1 and 2 in (a) and (b) indicate SiO_x NPs regions respectively, labels 3 and 4 indicate graphene film regions after the etch of SiO_x NPs, respectively. To identify changes in the surface chemistry, the deconvoluted EDS spectra were fitted to identify the elements of the final samples which would lead to a better understanding of the morphology of materials (see Table S2). The obtained Energy dispersive spectra of labels 1, 2 and 3 are shown in Figure 3c. As shown in figure, Cu was the substrate element. Besides, Si and O were found in 1 and 2. At the area of label 3, where there was no white dendritic structure, element C instead of Si was found, indicating the presence of graphene.

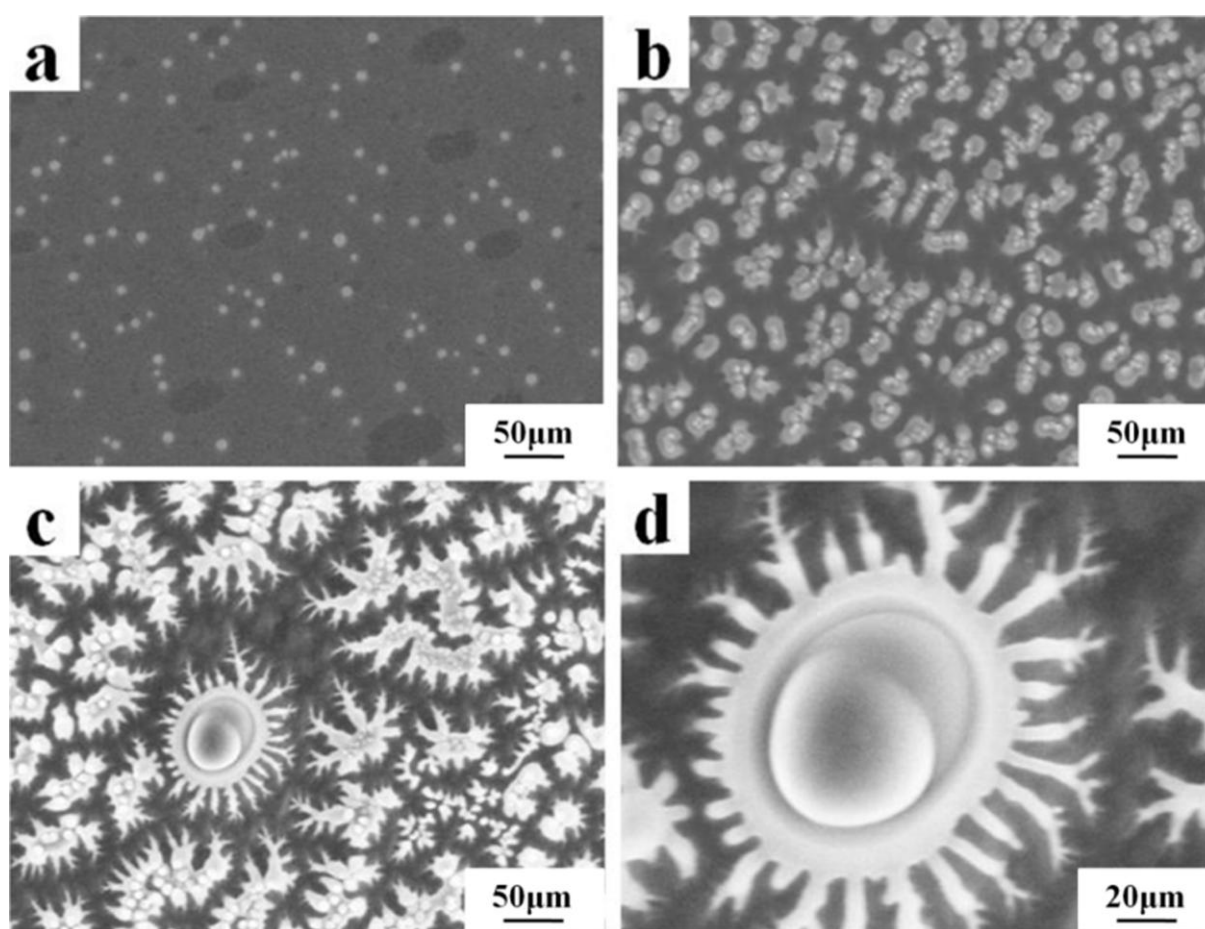


Figure 4. Evolution of SiO_x NPs patterns recorded on the same sample under the conditions for Figure 2d shown in Table S1.

Raman spectra of the areas labeled 1, 3 and 4 in Figure 3b were shown in Figure 3d. Raman spectra of graphene and other carbon materials can provide significant information regarding the carbon materials such as the phonon structure, electronic structure, and defect structure[34]. The spectra of 3 and 4 are characteristic of single-layer graphene (a sharply 2D peak located at 2690cm^{-1} with a full width at half-maximum of $42\text{-}55\text{ cm}^{-1}$ and a large intensity ratio of the 2D and G bands (

$I_{2D}/I_G=2.5-5$)), whereas 1 contains no graphene signal. The small peak located at 1450 cm^{-1} in the spectrum of 1 (as seen from embedded partial magnification) comes from the SiO_x , as confirmed by the presence of the same peak in the Raman spectrum of SiO_2 . The spectra of graphene only feature a couple of Raman active bands: G-band at 1580 cm^{-1} and the disorder band caused by the defects (D-band) at approximate 1350 cm^{-1} . Figure 3d shows the difference of D band of 3 and 4. I_G/I_D ratio of sample obtained from the graphene region was bigger than that from the graphene edge where was etched by SiO_x NPs, reflecting more defects at the etching area. The 2D peak in graphene is due to two phonons with opposite momentum in the highest branch[35], this peak changes wavenumbers with varying the scanning positions due to a double resonance process, which links the phonon wave vectors to the electronic band structure[36]. The up-shift of 2D peak in pattern 4 might be caused by the wrinkle of layer sheet. Meanwhile, the little up-shift of G peak4 compared with that in 3 was partially due to chemical doping.

From the above figures, it is enthralling to find that different growth patterns clearly exhibit the evolution from dots to branches or from simplification to fractal geometry in the actual experiments. For the abstraction of this SiO_x NPs growth mode testing, we further investigated the effect of temperature, concentrations of silica gel, growth time, and Ar/ H_2 flow rate ratios on morphology in the process.

Samples prepared under different concentrations of silica gel were in accordance with the Diffusion-limited Aggregation (DLA) process (as seen in Figure S1). At the first stage (30-60min, Figure 4b), particles seemed to be little rough after the projection of arm-like branches of spherical samples. Then random dendrites generated around the particles and grew as time passed. Interior branches, however, stopped growing due to their open neighborhood during the incubation period, suggesting the existence of screening effect. At the second stage (60-90min, Figure 4c), the particle pattern with diameter about $50-60\mu\text{m}$ was very similar to clusters produced through the two-dimensional (2D) DLA process. These particle patterns were analyzed and found to be self-similar two-dimensionally (Figure 4d). What's more, the variation of temperature from 1000 to $1060\text{ }^\circ\text{C}$ resulted in the same growth behavior in essence (Figure S2). Further increasing Ar/ H_2 ratio led to branches structure with lots of protruding arms, and these arms gradually became sharper with the whole structure more like flower (Figure S3). At last, the concentration of silica gel was discussed that with the increase of concentration, the sample lost its initial patterns (Figure S4).

4. CONCLUSIONS

SiO_x NPs accompanied with the formation of monolayer graphene which followed the DLA process have been successfully prepared by CVD method. Here we have demonstrated for the time that the morphology of SiO_x NPs can be controlled by changing experimental conditions like concentrations of silica gel, ratios of Ar/ H_2 flow rate and growth time. Two stages of the growth were characterized by (1) the projection of arm-like branches after the nucleation of SiO_x NPs and (2) the proceeding of two-dimensional self-similarity. The results show that etching and growing patterns of

particles shared characteristics of fractal geometry and the growth mode was a diffusion-controlled process.

SUPPORTING INFORMATION

Methods

50 μ m thick Cu foil (99.8% purity) was obtained from Hefei Crystal Technical Material Co. Ltd.

In method 1, the samples were first ultrasonically cleaned in weak acid and then spin-coated with different concentrations of silica gel at 2500 cycle/min followed by curing at 50 °C for 2h. After samples were loaded into the 80 mm quartz tube, the system was pumped from ambient pressure to ~15 Pa followed by filling the system with hydrogen gas and argon gas mixture. The process was repeated for several times to ensure that the reactor chamber contained the air as little as possible. After switching off pumping, the quartz tube kept at ambient pressure by the continuous feedstock of Ar/H₂ hydrogen. The furnace was then heated up to a desired temperature in about 1 h followed by keeping the sample in the Ar/H₂ ambience for 1-5 h. A monolayer graphene film with SiO_x NPs was then grown on the surface of the copper using CH₄ in Ar/H₂ as the carrier gas for different stage time (each stage was set for 30minutes). Finally, the sample was cooled rapidly to room temperature.

In method 2, after the formation of multilayer graphene on Cu foil, silica gel films were coated onto the graphene by spin coating and then heated at 50°C for 2h. After being located in the quartz tube, the samples were heated up to 1060°C with different Ar/H₂ flow rate ratios at ambient pressure. Finally, the samples were rapidly cooled to room temperature.

The obtained films were rinsed with distilled water for several times to remove any possible residues and then dried, finally transferred onto the substrate for further characterizations.

The samples were characterized by scanning electron microscopy (SEM, Hitachi S-4800, 1 kV), energy dispersive spectrum (EDS, Hitachi S-4800, 10 kV) and Raman spectroscopy (HORIBA, LabRAM HR Evolution, with laser excitation at 514 nm).

Table S1 Summary of graphene growth and etching conditions in Figure 2

Figure	Method	Ar/H ₂ (sccm)	Growth CH ₄ (sccm)	Growth Ar/H ₂ (sccm)	Growth time (min)	Silica gel concentration	Graphene layer	Temperature (°C)
2a	1	800/10	0.25	800/20	60	5% wt	Single	1060
2b	1	800/10	0.25	800/50	90	5% wt	Single	1060
2c	1	800/10	0.25	800/100	90	5% wt	Single	1060
2d	1	800/10	0.25	800/20	90	10% wt	Single	1060
2e	1	800/10	0.25	800/20	90	20% wt	Single	1060
2f	1	800/10	0.25	800/20	60	30% wt	Single	1060
2g	2	800/20	5	800/20	90	10% wt	Few	1060

2h	2	800/20	5	800/20	60	20% wt	Few	1060
2i	2	800/20	5	800/20	30	30% wt	Few	1060

To identify changes in the surface chemistry, the deconvoluted EDS spectra were fitted to identify the elements of the final samples which would lead to a better understanding of the morphology of materials.

Table S2 Elements percentage of sample in Figure 3.

Label 1.

Elements	Weight Percentage	Atomic Percent
O	2.39	8.74
Si	1.26	2.62
Cu	96.35	88.63
Total	100.00	

Label 2.

Elements	Weight Percentage	Atomic Percent
O	2.84	10.26
Si	1.24	2.54
Cu	95.92	87.19
Total	100.00	

Label 3.

Elements	Weight Percentage	Atomic Percent
C	3.06	14.32
Cu	96.94	85.68
Total	100.00	

The amorphous SiO_x NPs can be monitored by SEM. The trend is remarkably correspondent in the evolution of the graphene crystal. The first growth stage is the nucleation of SiO_x (Figure S1a). The second one around the ambient temperature (double-diffusion technique) which starts on the base of first stage is characterized by the formation of elongated hexagonal-prismatic seeds followed by the growth of self-similar concentric shells, including the elongated prismatic branching (fractal growth). This stage ends up with the formation of anisotropic units with nearly parallel orientation (maximum spherical aggregates).

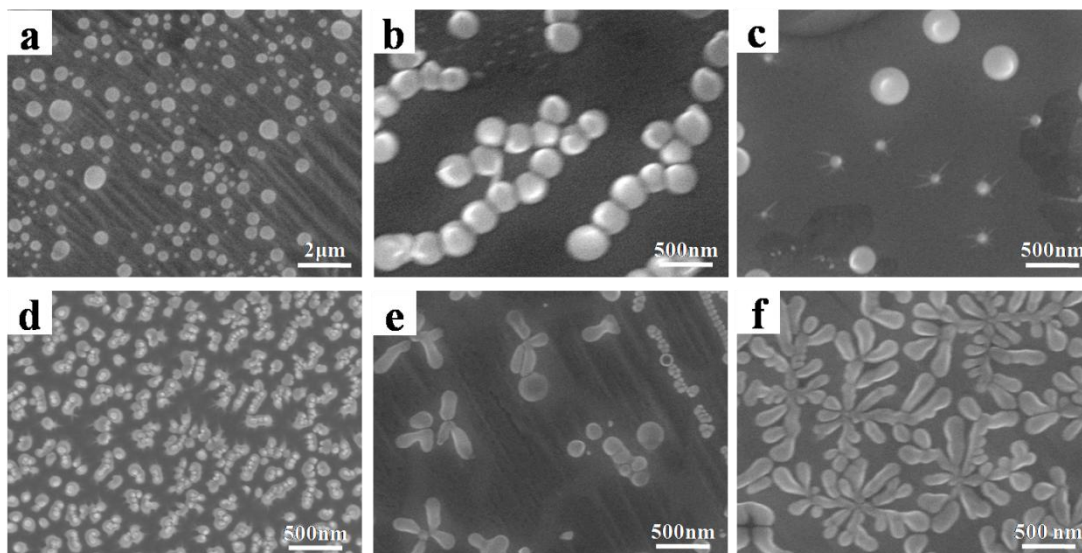


Figure S1. SEM of samples prepared in accordance with the DLA process in different stages: (a) after 5 min, (b) after 10min, (c) after 15 min, (d) after 30 min, (e) after 60 min and (f) after 90 min growth.

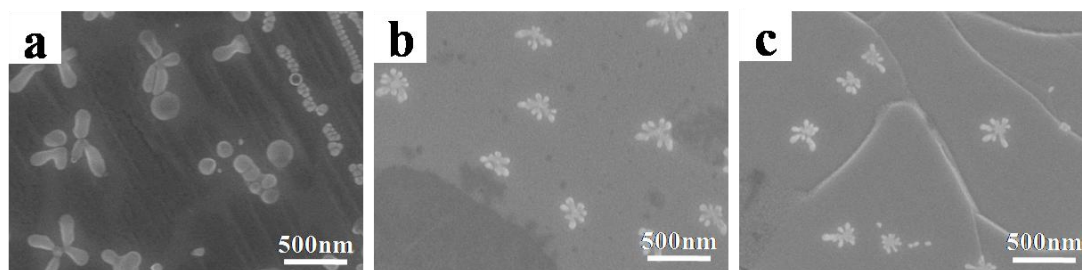


Figure S2. SEM of samples prepared in accordance with the DLA process at different temperatures: (a) 1000°C, (b) 1030°C And (c) 1060°C.

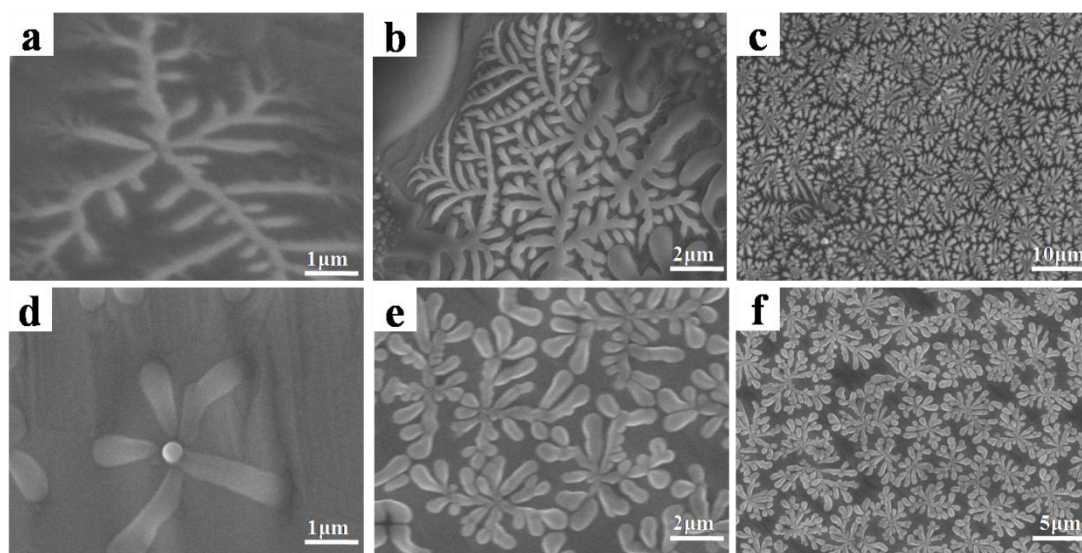


Figure S3. SEM of samples prepared in accordance with the DLA process with different Ar/H₂ ratio at (a) 800/100, (b) 800/80, (c) 800/60, (d) 800/40, (e) 800/20 and (f) 800/10.

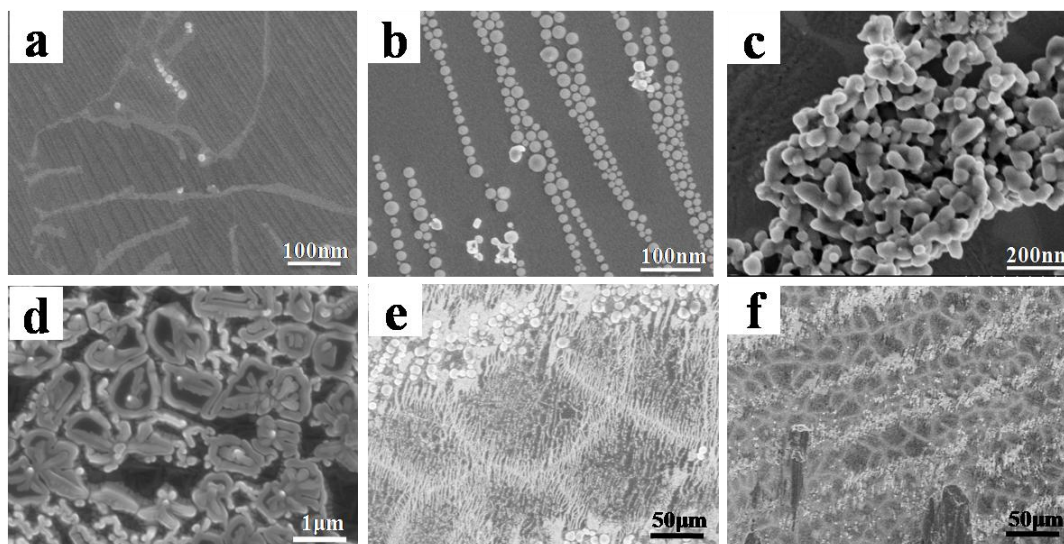


Figure S4. SEM of samples prepared with different concentrations of silica gel at (a)1% wt , (b)3% wt , (c)10%wt and (d)30% wt accompany with monolayer graphene production; (e)20% wt and (f)30%wt accompany with multilayer graphene production.

ACKNOWLEDGMENTS

The authors would like to thank Luo Shufang of Centre of Materials Science at NUDT for excellent technical support and Professor Chu Zengyong for critically reviewing the manuscript.

Reference

1. R. Carius, R. Fischer, E. Holzenkämpfer, J. Stuke, *Journal of Applied Physics* 52 (1981) 4241.
2. B. Du Ahn, Y.G. Ko, S.H. Oh, J.-H. Song, H.J. Kim, *Thin Solid Films* 517 (2009) 6414.
3. W.K. Lee, E.J. Kim, S.H. Hahn, *Vacuum* 85 (2010) 30.
4. M. Kawasaki, T. Tsukamoto, H. Yamane, *FIBER* 58 (2002) 29.
5. T. Kiguchi, N. Wakiya, K. Shinozaki, N. Mizutani, *Integrated Ferroelectrics* 51 (2003) 51.
6. A. Milutinovic, Z. Dohcevic-Mitrovic, D. Nesheva, M. Scepanovic, M. Grujic-Brojcin, Z. Popovic, *Trans Tech*, (2007)309.
7. T.-Y. Lin, L.-M. Chen, S.-C. Chang, T.-S. Chin, *Applied Physics Letters* 95 (2009) 2105.
8. Y.-H. Pai, C.-H. Chang, G.-R. Lin, *IEEE Journal of* 15 (2009) 1387.
9. D.B. Farmer, H.-Y. Chiu, Y.-M. Lin, K.A. Jenkins, F. Xia, P. Avouris, *Nano letters* 9 (2009) 4474.
10. C. Mattevi, H. Kim, M. Chhowalla, *Journal of Materials Chemistry* 21 (2011) 3324.
11. M.D. Stoller, S. Park, Y. Zhu, J. An, R.S. Ruoff, *Nano letters* 8 (2008) 3498.
12. X. Xiao, T.E. Beechem, M.T. Brumbach, T.N. Lambert, D.J. Davis, J.R. Michael, C.M. Washburn, J. Wang, S.M. Brozik, D.R. Wheeler, *Acs Nano* 6 (2012) 3573.
13. R. Sengupta, M. Bhattacharya, S. Bandyopadhyay, A.K. Bhowmick, *Progress in polymer science* 36 (2011) 638.
14. T. Vicsek, *World Scientific*(1992).
15. A. Ghosh, R. Batabyal, G. Das, B. Dev, *AIP Advances* 6 (2016) 015301.
16. D.H. Jung, C. Kang, J.E. Nam, H. Jeong, J.S. Lee, *Scientific Reports* 6 (2016) 21136.
17. Y. Yang, J. Zeng, A. Volland, J. Blandin, S. Gravier, C.T. Liu, *Acta Materialia* 60 (2012) 5260.
18. A. Dawar, A. Chandra, *Physics Letters A* 378 (2014) 2951.
19. D. Nieckarz, P. Szabelski, *Chemical Communications* 50 (2014) 6843.
20. J.A. Kaandorp, *Springer Science & Business Media* 2012.

21. P. Xu, X. Han, B. Zhang, Y. Du, H.-L. Wang, *Chemical Society Reviews* 43 (2014) 1349.
22. S. Havlin, S. Buldyrev, A. Goldberger, R. Mantegna, S. Ossadnik, C.-K. Peng, M. Simons, H. Stanley, *Solitons & Fractals* 6 (1995) 171.
23. B.B. Mandelbrot, *Annals of the New York Academy of Sciences* 357 (1980) 249.
24. L. Pietronero, A. Erzan, C. Evertsz, *Physical review letters* 61 (1988) 861.
25. Y. Zheng, Z. Zhang, P. Guo, P. He, Z. Sun, *Journal of Solid State Chemistry* 184 (2011) 2114.
26. D. Geng, B. Wu, Y. Guo, B. Luo, Y. Xue, J. Chen, G. Yu, Y. Liu, *Journal of the American Chemical Society* 135 (2013) 6431.
27. S.S. Datta, D.R. Strachan, S.M. Khamis, A.C. Johnson, *Nano letters* 8 (2008) 1912.
28. Z. Zhang, M.G. Lagally, *Science* 276 (1997) 377.
29. Z. Zhang, F. Wu, H. Zandvliet, B. Poelsema, H. Metiu, M. Lagally, *Physical review letters* 74 (1995) 3644.
30. H. Roder, E. Hahn, H. Brune, J.-P. Bucher, K. Kern, *Nature* 366 (1993) 141.
31. J.-M. Pin, N. Sbirrazzuoli, L. Sacarescu, A. Mija, *Polymer Chemistry* (2016).
32. Z. Zhang, X. Chen, M.G. Lagally, *Physical review letters* 73 (1994) 1829.
33. A. Krasheninnikov, P. Lehtinen, A.S. Foster, P. Pyykkö, R.M. Nieminen, *Physical review letters* 102 (2009) 126807.
34. S. Hang, Z. Moktadir, H. Mizuta, *Carbon* 72 (2014) 233.
35. S. Piskanec, M. Lazzeri, F. Mauri, A.C. Ferrari, J. Robertson, *Physical Review Letters* 93 (2004) 185503.
36. C. Thomsen, S. Reich, *Physical Review Letters* 85 (2000) 5214.

© 2016 The Authors. Published by ESG (www.electrochemsci.org). This article is an open access article distributed under the terms and conditions of the Creative Commons Attribution license (<http://creativecommons.org/licenses/by/4.0/>).